Hindawi
Adsorption Science & Technology
Volume 2021, Article ID 3131309, 8 pages
https://doi.org/10.1155/2021/3131309

Research Article

Effect of Ce Addition on Adsorption and Oxidation of NO over MnO_x/Al_2O_3

Chunhui Mou,[1] **Hui Li**,[2] **Ning Dong**,[2] **Shien Hui**,[2] **and Denghui Wang**[2]

[1]*School of Electronic and Information Engineering, Xi'an Jiaotong University, Xi'an 710049, China*
[2]*School of Energy and Power Engineering, Xi'an Jiaotong University, Xi'an 710049, China*

Correspondence should be addressed to Denghui Wang; denghuiwang@163.com

Received 31 May 2021; Revised 21 August 2021; Accepted 26 August 2021; Published 8 September 2021

Academic Editor: Stefano Salvestrini

The MnO_x/Al_2O_3 catalysts with different Ce content doping were prepared by an ultrasonic impregnation method, and the catalytic activity for NO oxidation removal was tested in a fixed-bed quartz tube furnace. Simultaneously, the catalysts were characterized by X-ray diffraction (XRD), X-ray photoelectron spectroscopy (XPS), full-automatic physical-chemical adsorption instrument, and field emission scanning electron microscope (FESEM) to analyze the effect of Ce addition on the adsorption capacity and catalytic activity. Experimental results validated that the activity of the MnO_x/Al_2O_3 catalyst was greatly promoted with Ce addition. According to the characterization results, it could be concluded that Ce doping led to significant changes in the crystalline phase on the catalyst surface, which increased the relative content of surface lattice oxygen and promoted the catalytic oxidation of NO. By observing the physical properties of the surface and analyzing the surface elements of the catalyst, it could be inferred that a manganese-cerium solid solution was formed on the surface of $Mn_{0.4}Ce_{0.05}/Al$. Moreover, Ce addition increased the catalyst pore size, which enhanced the adsorption and contact of NO and O_2 with the active sites on the catalyst surface, and reduced the resistance of the reactants during internal diffusion. All these variations assigned to $Mn_{0.4}Ce_{0.05}/Al$ were favorable for the catalytic oxidation of NO.

1. Introduction

The combustion of massive fossil fuels brings about the harmful emission of nitrogen oxides (NO_x). The problem has attracted great attention in recent decades, for the close relationship between NO_x and many serious environmental issues, including acid rain, city photochemical smog, and tropospheric ozone depletion [1–4]. To reduce the poisonous NO_x emissions, many techniques have been researched and applied to thermal power plants and diesel engines. Reductive denitration technology has been extensively researched, including selective catalytic reduction (SCR) and selective noncatalytic reduction (SNCR). Due to its high efficiency, SCR has always been regarded as an effective method to remove fixed emission sources such as power plants [5–8]. In the common SCR process, injected NH_3 reduces noxious NO_x to harmless N_2 with the aid of efficient catalysts. The typical reactions are as follows [9, 10].

$$\text{Standard SCR}: 4NH_3 + 4NO + O_2 \longrightarrow 4N_2 + 6H_2O \quad (1)$$

$$\text{Fast SCR}: 2NH_3 + NO + NO_2 \longrightarrow 2N_2 + 3H_2O \quad (2)$$

NH_3-SCR has also exposed many problems in a wide range of industrial applications, such as high investment and operating costs, NH_3 escape, N_2O generation, and catalyst deactivation [11, 12]. The greenhouse effect of N_2O is up to 300 times that of carbon dioxide. The almost inevitable escape of NH_3 is particularly worrying. It not only increases the operation cost but also easily results in serious air preheater blocking. Therefore, how to remove NO_x from coal-burning exhaust gas with low cost, pollution-free, and high

efficiency has become a research focus. Recently, NO catalytic oxidation removal is drawing much attention for its getting rid of NH_3 during NO_x removal [13–15]. Although over 90% of NO_x formed in fuel combustion is insoluble NO, its oxidation product NO_2 is rather soluble. Therefore, with the participation of catalysts, it is feasible to use the remaining O_2 in the flue gas to oxidize NO to NO_2, which is then captured by alkali liquor in a wet flue gas desulfurization plant [11, 16, 17].

Although many noble metal catalysts have shown good performance in NO catalytic oxidation, the high cost limits their wide application in coal-fired power plants [18–20]. Transition metal oxides have been proven with excellent performance compared to noble metal catalysts, with a wide range of sources, low prices, simple preparation processes, and good thermal stability. Therefore, they have received extensive and in-depth research in recent years [21–23]. Wu et al. prepared a series of MnO_x/TiO_2 composite nanoxides by deposition-precipitation method, and the sample with the Mn/Ti ratio of 0.3 showed a superior activity for NO oxidation, reaching 89% at 250°C [24]. Mn-based catalysts impregnated on TiO_2 with different crystalline phases were studied by An et al. for the oxidation of NO to NO_2, and 10% MnO_x/TiO_2 exhibited the highest efficiency 83% at 300°C [22]. The NO oxidation on Cu_2O with molecular oxygen, dissociated oxygen, and lattice oxygen was studied by Sun et al. using periodic density functional theory, and the Eley-Rideal mechanism was favored to explain the catalytic effect of Cu_2O on NO oxidation [25].

Active Al_2O_3 has the characteristics of large adsorption capacity, large specific surface area, good thermal stability, nontoxicity, and noncorrosiveness. Therefore, it is regarded as an excellent catalyst support material and has received extensive attention in the field of catalysis. Wang et al. [26] used a sol-gel method to prepare a series of Ce-based catalysts, selecting Co, Mn, Fe, Cr, and Ni as the doping metal elements. At a reaction temperature of 230°C, the order of NO catalytic activity is Co > Mn > Cr > Ni > Fe.

Although much work has been carried out on NO catalytic oxidation over transition metal oxides, there are some deficiencies along with these studies [21–25]. Firstly, only oxidation efficiency but not removal efficiency was focused on during the experiments. Secondly, the temperature window of the researched catalysts was relatively narrow, not suitable for large-scale practical application. In this investigation, we prepared a series of MnO_x/Al_2O_3 and Ce-doped MnO_x-CeO_y/Al_2O_3 catalysts and investigated the oxidation denitration performance of these catalysts. The effect of Ce doping on the catalyst physicochemical properties was discussed, and microcharacterization analysis was carried out to explore the key points affecting efficiency.

2. Experimental

2.1. Catalyst Preparation. All tested samples in the study were prepared via an ultrasonic impregnation method. Chemicals used here were of analytical grade. Firstly, 0.04 mol (10.04 g) $Mn(NO_3)_2{\cdot}4H_2O$ was dissolved in 20 mL deionized water. Afterwards, with continuous magnetic stirring, 0.1 mol (10.20 g) Al_2O_3 was added into the solution (particle size = 20 nm; specific surface area ≥ 160 m^2/g). Then, the mixture experienced an ultrasonic oscillation lasting for 0.5 h to help to uniformly mix. After standing at room temperature overnight, the suspension was dried in an oven at 105°C for 12 h. The obtained solid product was calcined at 600°C for 5 h and then crushed and sieved to 60-80 mesh. Because the molar ratio of added Mn and Al was 0.4 in the sample, it was denoted as $Mn_{0.4}/Al$.

For samples with different Ce addition, a specific amount (0.005 mol, 0.01 mol, and 0.02 mol, respectively) of $Ce(NO_3)_3{\cdot}6H_2O$ was dissolved in deionized water with $Mn(NO_3)_2{\cdot}4H_2O$ together in the first preparation step. Other preparation procedures were the same as mentioned above. The finally prepared samples were denoted as $Mn_{0.4}Ce_{0.05}/Al$, $Mn_{0.4}Ce_{0.1}/Al$, and $Mn_{0.4}Ce_{0.2}/Al$, respectively.

2.2. Catalytic Activity Test. The catalyst activity test system is shown in Figure 1. The catalytic activity test was carried out in a fixed-bed quartz tube furnace. 0.5 g sample was fixed on the bottom of the quartz glass tube by quartz wool. The total gas flow rate was fixed to 1 L/min (STP), with 600 ppm NO, 8 vol% O_2, and balanced N_2. The exhaust gas after the reaction at a certain temperature was introduced into a 0.5 mol/L sodium hydroxide aqueous solution for absorption, after which the outlet gas composition was examined online by a Fourier transform infrared spectroscopy gas analyzer (Gasmet DX4000, Finland).

The NO removal efficiency was calculated according to the following equation:

$$\text{NO removal efficiency}\,(\%) = \left(1 - \frac{[\text{NO}]_{\text{out}} + [\text{NO}_2]_{\text{out}}}{[\text{NO}]_{\text{in}}}\right) \times 100. \tag{3}$$

2.3. Catalyst Characterization. N_2 adsorption-desorption measurement was performed on a full-automatic physical-chemical adsorption instrument (Micromeritics ASAP2020, USA) to determine the textural properties of samples. The specific surface area was acquired by the Brunauer-Emmett-Teller (BET) method, while the total pore volume and mean pore diameter were obtained according to the Barrett-Joyner-Halenda (BJH) method. The micromorphologies of samples were monitored by a field emission scanning electron microscope (FESEM, GeminiSEM 500, Germany). An X-ray diffraction (XRD) meter (Xpert pro, Netherlands) was adopted to identify the crystal phases of samples. The scanning angular velocity was 7°/min, and the scanning angle range was 20°-80°. An X-ray photoelectron spectroscopy (XPS, AXIS ULtrabld, UK) was employed to analyze the catalyst surface atomic concentrations, using C1s at 284.8 eV as the calibration.

3. Results and Discussion

3.1. Catalytic Activity. 600 ppm NO, 8 vol% O_2, and balanced N_2 were introduced into the reactor to explore the performance of catalysts with different contents of active component Ce (Figure 2). As the reaction temperature increased

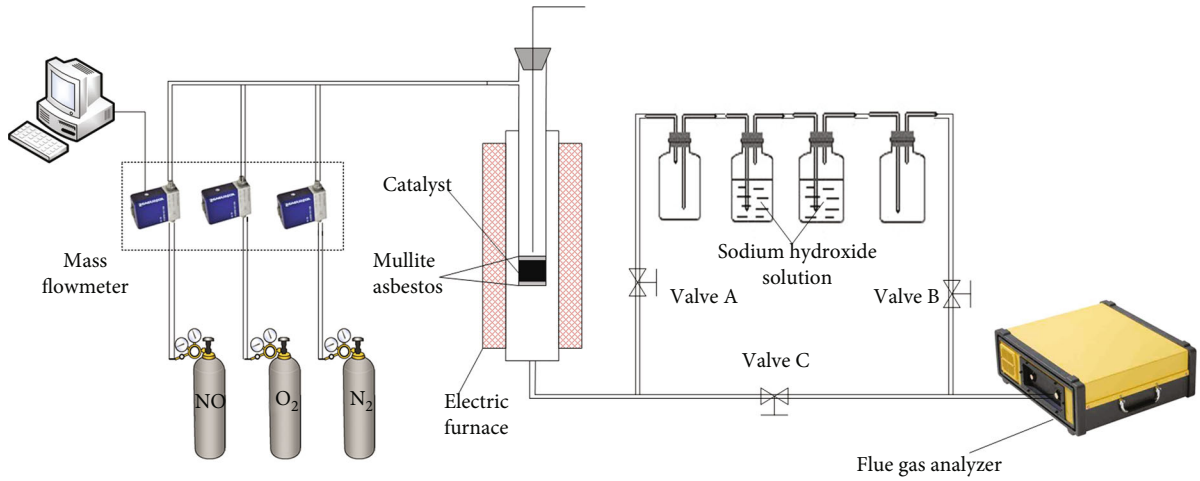

Figure 1: Schematic diagram of the experimental setup.

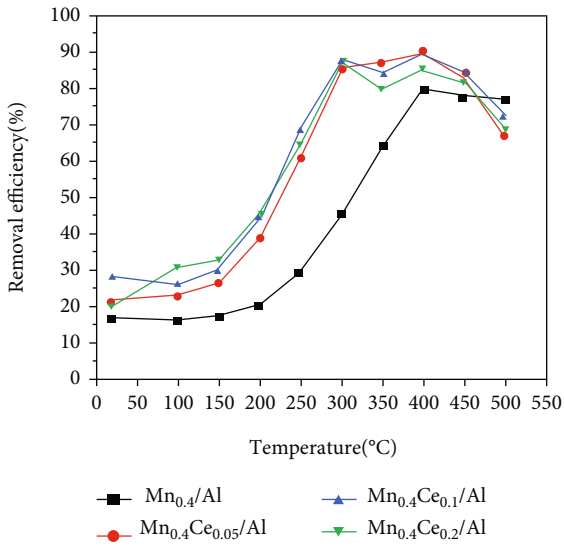

Figure 2: Removal efficiency of catalysts with different Ce contents.

from 20°C to 500°C, the NO removal efficiency was peaked at 400°C for all samples. The oxidation of NO to NO_2 is exothermic, and the reaction is limited by the thermodynamic equilibrium: the temperature rises, and the equilibrium shifts to the left. Therefore, the temperature increased, the NO oxidation rate decreased, and the denitration efficiency decreased. It was apparent that the removal efficiency of the Ce-doped $Mn_{0.4}$/Al catalyst was higher than that of the Ce-free $Mn_{0.4}$/Al catalyst, indicating the promotion effect of Ce addition on NO oxidation removal. In addition, the temperature window of $Mn_{0.4}Ce_x$/Al catalyst is wider than that of $Mn_{0.4}$/Al. The denitration efficiency of $Mn_{0.4}Ce_x$/Al at 300-450°C can be above 80%.

For the $Mn_{0.4}$/Al catalyst without Ce addition, the denitration efficiency increased gradually with the reaction temperature in 20-400°C, but it started to decrease slightly as the reaction temperature increased from 400°C to 500°C. The highest efficiency reached 79.5% at 400°C. When the molar ratio of Mn, Ce, and Al was 0.4 : 0.05 : 1, the efficiency reached the highest peak of 89.5%. When the molar ratio of Mn, Ce, and Al was 0.4 : 0.1 : 1, the efficiency peak reached 89.1%, similar to $Mn_{0.4}Ce_{0.05}$/Al. For $Mn_{0.4}Ce_{0.2}$/Al, the highest efficiency was 85.2%, a little lower than $Mn_{0.4}Ce_{0.05}$/Al and $Mn_{0.4}Ce_{0.1}$/Al. Doping with Ce improves the activity of the Mn/Al catalyst significantly. The temperature window moves to the left, indicating that the low-temperature activity of the catalyst is enhanced. Free Ce has excellent oxygen storage capacity, and a small amount of Ce doping increases the active sites on the catalyst surface, thereby increasing the NO removal rate. But excessive doping may aggravate the accumulation of surface crystals, cover some active centers, or block the pores, resulting in a decrease in the catalytic activity of the catalyst [27, 28]. In the subsequent surface analysis, it was found that after Ce doping, the specific surface area was significantly reduced. The active ingredient is not as much as possible and should be lower than the surface dispersion threshold. Otherwise, Ce agglomerates and stacks on the surface, so $Mn_{0.4}Ce_{0.05}$/Al with better activity is selected as the main research object in the follow-up.

3.2. XRD. The XRD patterns of $Mn_{0.4}$/Al and $Mn_{0.4}Ce_{0.05}$/Al expressing the crystal phases on the catalyst surface are depicted in Figure 3. MnO_x and CeO_x are the main research objects, so the Al_2O_3 carrier is not shown in Figure 3. There were only diffraction peaks corresponding to Mn_2O_3 in the XRD patterns of $Mn_{0.4}$/Al, indicating the well-crystallized Mn_2O_3 for $Mn_{0.4}$/Al catalysts. As for $Mn_{0.4}Ce_{0.05}$/Al, the diffraction peaks at 28.8°, 41.2°, and 67.2° were attributed to MnO_2, while the diffraction peaks at 28.9°, 36.5°, and 57.8° were ascribed to Mn_3O_4.

In the XRD patterns of $Mn_{0.4}Ce_{0.05}$/Al, the diffraction peaks of MnO_2 and Mn_3O_4 were very weak, and no diffraction peaks of Mn_2O_3 existed, which revealed that the addition of Ce had a great influence on the crystal structure of $Mn_{0.4}$/Al catalyst. It is worth noting that we also did not detect the crystalline phase of Ce in the XRD pattern, which indicated that Ce was evenly dispersed on the surface of the catalyst, or Ce enters the lattice of manganese. We speculate

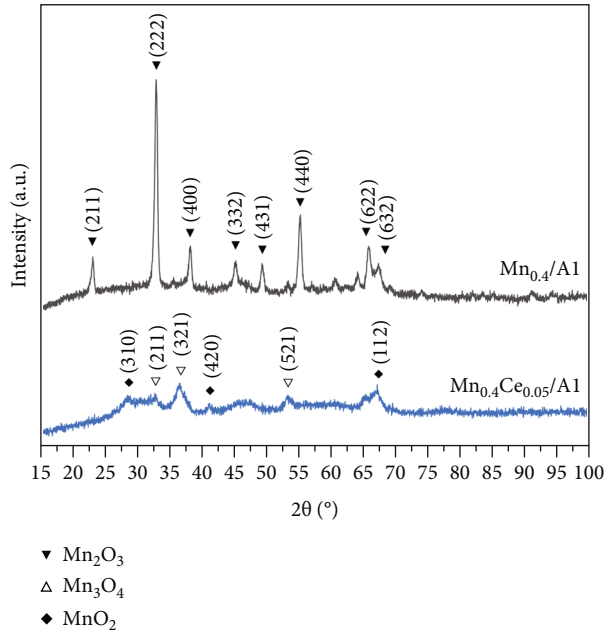

FIGURE 3: XRD patterns of $Mn_{0.4}$/Al and $Mn_{0.4}Ce_{0.05}$/Al.

that Ce atoms may enter the lattice of Mn_2O_3, resulting in the disappearance of a large amount of Mn_2O_3 crystal structure on the catalyst surface and resulting in the increase of the crystal structure of MnO_2 and Mn_3O_4 on the catalyst surface.

After adding active component Ce to $Mn_{0.4}$/Al catalyst, manganese and cerium interacted in a solid solution manner, and manganese ions entered the cerium oxide lattice to increase the oxygen storage capacity of the cerium oxide and the oxygen migration activity of the surface oxide [29]. This interaction was related to the electron transfer between manganese and cerium and the gain and loss of oxygen, and it also influenced the crystal structure of the catalyst and the valence state of manganese and cerium compounds. Therefore, related characterization analysis was carried out.

3.3. XPS. The XPS spectra for Mn 2p of $Mn_{0.4}$/Al and $Mn_{0.4}Ce_{0.05}$/Al are separately drawn in Figure 4(a) and Figure 4(b). Mn2p peaks for Mn oxides have many multiplet-split components, and the binding energy of Mn^{4+} is greater than Mn^{3+} [30]. In Figure 4(a), the binding energy peaks of 641.0 eV and 652.5 eV represent Mn^{3+}; the binding energy peaks at 642.8 eV and 653.4 eV represent Mn^{4+}. The relative size of the energy spectrum peak area represents the relative content of different manganese oxides on the catalyst surface. The $Mn^{4+}/(Mn^{3+} + Mn^{4+})$ ratio and the $Mn^{3+}/(Mn^{3+} + Mn^{4+})$ ratio were 46.1% and 53.9%, respectively.

On $Mn_{0.4}Ce_{0.05}$/Al, the binding energy peaks of 641.3 eV and 652.8 eV represent Mn^{3+}; the binding energy peaks at 642.8 eV and 654.2 eV represent Mn^{4+} in Figure 4(b). Compared with Mn0.4Ce0.05/Al, the energy level was shifted upward. The $Mn^{4+}/(Mn^{3+} + Mn^{4+})$ ratio and the $Mn^{3+}/(Mn^{3+} + Mn^{4+})$ ratio were 31.0% and 69.0%, respectively. The

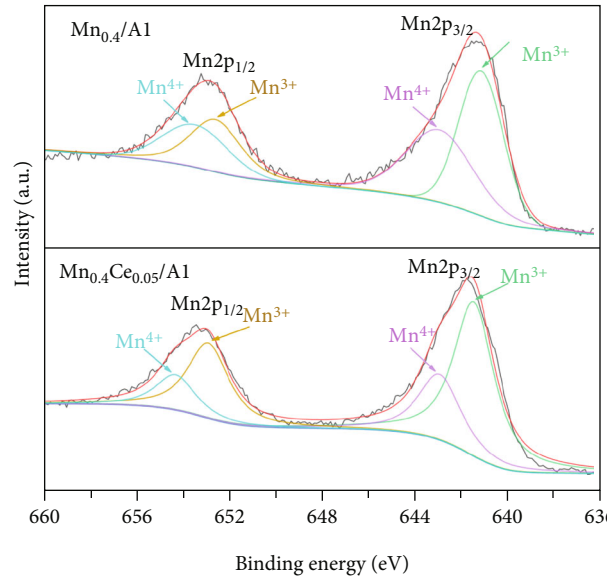

FIGURE 4: XPS spectra for Mn 2p of (a) $Mn_{0.4}$/Al and (b) $Mn_{0.4}Ce_{0.05}$/Al.

results indicated that partial Mn^{4+} converted to Mn^{3+} as a result of the addition of cerium. The increase of Mn^{3+} and the decrease of Mn^{4+} favored the catalyst oxidation activity, which was consistent with the results of Atribak et al. [31]. They also confirmed that the activity of Mn^{4+} for NO oxidation was lower than that of Mn^{3+}.

Figure 5 shows the XPS spectra for O 1s of $Mn_{0.4}$/Al (Figure 5(a)) and $Mn_{0.4}Ce_{0.05}$/Al (Figure 5(b)). There were two kinds of oxygen in catalysts, i.e., surface absorbed oxygen (denoted as O_α) and lattice oxygen (denoted as O_β). In

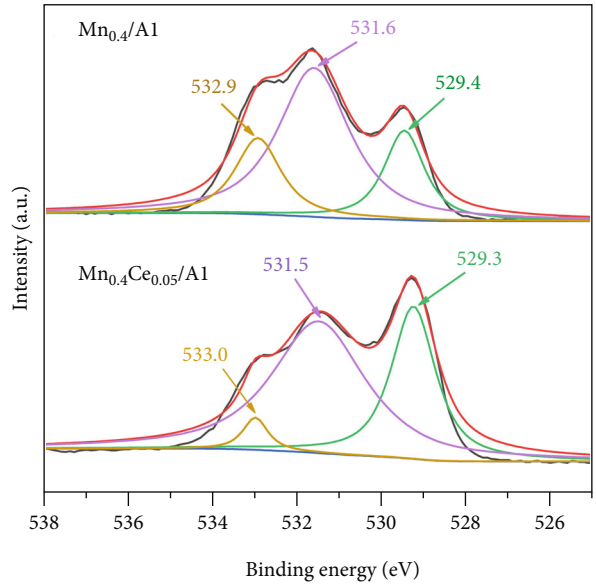

Figure 5: XPS spectra for O 1s of (a) the $Mn_{0.4}$/Al catalyst and (b) the $Mn_{0.4}Ce_{0.05}$/Al catalyst.

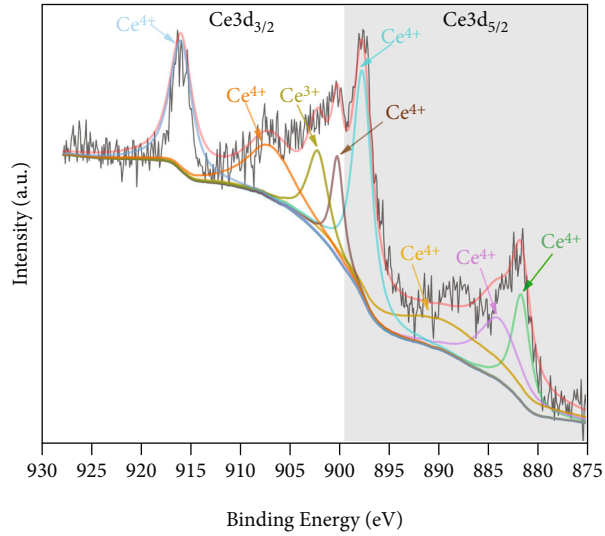

Figure 6: XPS spectra for Ce 3d of the $Mn_{0.4}Ce_{0.05}$/Al catalyst.

Table 1: Results of the XPS results of $Mn_{0.4}$/Al and $Mn_{0.4}Ce_{0.05}$/Al.

Sample	$Mn^{4+}/(Mn^{3+} + Mn^{4+})$	$Mn^{3+}/(Mn^{3+} + Mn^{4+})$	O_α/O	O_β/O
$Mn_{0.4}$/Al	46.1%	53.9%	79.6%	20.4%
$Mn_{0.4}Ce_{0.05}$/Al	31.0%	69.0%	65.7%	34.3%

Figure 5(a), peaks at 532.9 and 531.6 eV were attributed to O_α, while the peak at 529.4 eV corresponded to O_β. And in Figure 5(b), peaks at 533.0 and 531.5 eV were attributed to O_α, while the peak at 529.3 eV corresponded to O_β. Although the binding energy for each peak showed few differences in Figure 5(a) and Figure 5(b), the intensity varied greatly, especially the relative intensity of O_α and O_β. The proportion of O_β to $(O_\alpha + O_\beta)$ in Figure 5(a) was as low as 20.4%, whereas the proportion in Figure 5(b) increased to 34.3%.

Table 2: Physical properties of catalysts.

Sample	BET surface area (m^2/g)	BJH pore volume (cm^3/g)	Average pore diameter (nm)
$Mn_{0.4}$/Al	86.61	0.143	23.17
$Mn_{0.4}Ce_{0.05}$/Al	69.44	0.139	28.69

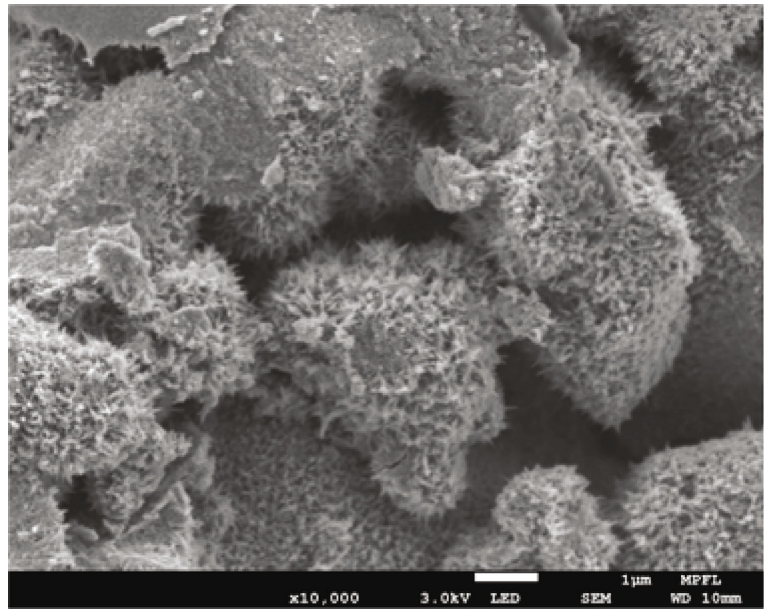

(a)

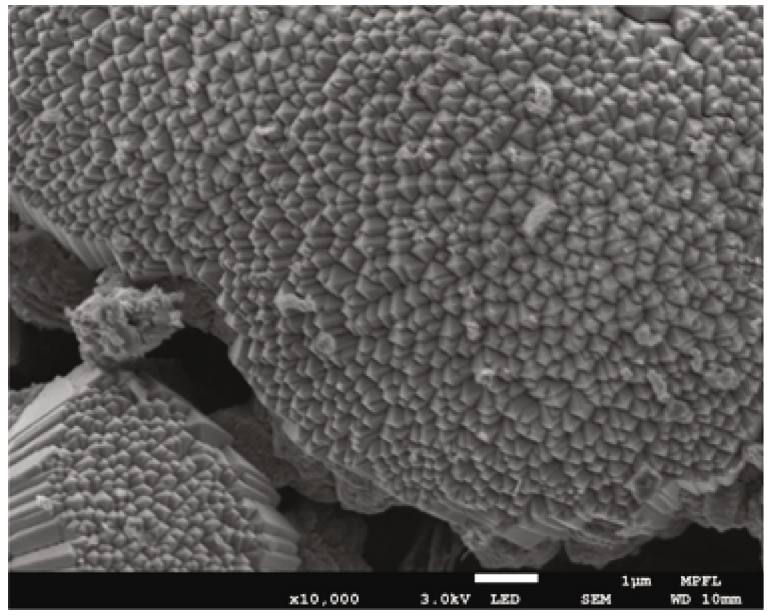

(b)

Figure 7: FESEM images of (a) $Mn_{0.4}$/Al and (b) $Mn_{0.4}Ce_{0.05}$/Al.

Lattice oxygen played an important role in NO oxidation. After adsorption on the catalyst surface, NO was first oxidized by the active lattice oxygen to form nitrite or nitrate on the surface of the catalyst [32]. The higher proportion of O_β signified the more lattice oxygen in catalysts, so $Mn_{0.4}Ce_{0.05}$/Al exhibited better catalytic oxidation activity than $Mn_{0.4}$/Al. Xiang et al. [33] built a model of manganese oxide loaded on alumina and analyzed the adsorption of NO and O_2 on the Mn/Al surface by density functional theory. Calculations have found that O_2 is not easy to stably adsorb on the Mn/Al surface, so the surface lattice oxygen O_β is more likely to participate in the oxidation of NO by the MvK mechanism. This was consistent with our experimental conclusions that the $Mn_{0.4}Ce_{0.05}$/Al catalyst with higher lattice oxygen content had a stronger ability to oxidize NO.

Figure 6 shows the XPS spectra for Ce 3d of $Mn_{0.4}Ce_{0.05}$/Al. The Ce 3d spectrum consists of two series of spin-orbit lines $Ce3d_{3/2}$ and $Ce3d_{5/2}$ [34]. There were eight distinct characteristic peaks, of which the peaks at 881.8 eV, 889.2 eV, 897.7 eV, 902.3 eV, 907.0 eV, and 916.0 eV correspond to Ce^{4+} [26, 35], and the peaks at 902.2 eV and 884.0 eV correspond to Ce^{3+} [36, 37]. It indicated that Ce in $Mn_{0.4}Ce_{0.05}$/Al had two forms of Ce^{4+} and Ce^{3+} after calcination at high temperature. The $Ce^{4+}/(Ce^{3+}$

$+ Ce^{4+}$) ratio and the $Ce^{3+}/(Ce^{3+} + Ce^{4+})$ ratio were 20.56% and 79.44%, respectively.

Ce had strong oxygen storage capacity and stores and releases oxygen through the transformation of Ce^{3+} and Ce^{4+}, which was consistent with the higher lattice oxygen content on the surface of $Mn_{0.4}Ce_{0.05}$/Al. It can be seen from Figure 1 that Ce doping improved the low-temperature activity of the catalyst, which was consistent with the study of other scholars [38, 39]. In addition, the doping of Ce element led to a reduction in the amount of O atoms combined with Mn, which in turn converted Mn^{4+} to Mn^{3+} with better activity.

The results of the XPS characteristics of $Mn_{0.4}$/Al and $Mn_{0.4}Ce_{0.05}$/Al are listed in Table 1. According to the analysis above, the increase of Mn^{3+} and lattice oxygen was important for the effective improvement of catalyst activity.

The physical properties of $Mn_{0.4}$/Al and $Mn_{0.4}Ce_{0.05}$/Al are listed in Table 2, mainly including the BET surface area, the BJH pore volume, and the BJH average pore diameter. From Table 2, it could be found that the surface area and the pore volume of the $Mn_{0.4}Ce_{0.05}$/Al catalyst were lower than those of the $Mn_{0.4}$/Al catalyst. On the contrary, the pore diameter of the $Mn_{0.4}Ce_{0.05}$/Al catalyst was higher.

According to the XRD analysis results, cerium ions entered the manganese oxide lattice, resulting in an increase in the weight per unit volume of the pore structure and resulting in the decrease in the specific surface area and pore volume of the catalyst [40]. And it could be found in Table 1 that the O_α of $Mn_{0.4}Ce_{0.05}$/Al catalyst was less than that of $Mn_{0.4}$/Al. The decrease of O_α was probably because of the decrease of the catalyst pore volume. Larger pore size will enhance the contact of NO and O_2 with the active sites on the catalyst surface and reduce the resistance of the reactants during internal diffusion, so $Mn_{0.4}Ce_{0.05}$/Al exhibits stronger NO removal performance.

3.4. FESEM. The FESEM images with magnification times (×10000) of $Mn_{0.4}$/Al and $Mn_{0.4}Ce_{0.05}$/Al are shown in Figure 7. As shown in Figure 7(a), the $Mn_{0.4}$/Al surface was evenly distributed with fine particles. According to the above XRD analysis results, they were likely to be Mn_2O_3 particles. As shown in Figure 7(b), there were many needle-like substances on the $Mn_{0.4}Ce_{0.05}$/Al surface. The surface of $Mn_{0.4}Ce_{0.05}$/Al was rougher, which was conducive to generating more active sites and also conducive to the adsorption of reactants, which strengthens the catalytic oxidation of NO on the surface.

4. Conclusions

The NO oxidation removal activity of $Mn_{0.4}$/Al catalysts with different Ce contents ($Mn_{0.4}$/Al, $Mn_{0.4}Ce_{0.05}$/Al, $Mn_{0.4}Ce_{0.1}$/Al, and $Mn_{0.4}Ce_{0.2}$/Al) was studied experimentally. The results showed that the activity of $Mn_{0.4}$/Al catalysts was effectively promoted with Ce addition, and the $Mn_{0.4}Ce_{0.05}$/Al performed the best.

Simultaneously, the physical-chemical properties and microstructures of $Mn_{0.4}$/Al and $Mn_{0.4}Ce_{0.05}$/Al were compared and analyzed by various characterization methods, which was helpful to reveal the mechanism of catalytic oxidation of NO by Mn-based catalysts and the effect of Ce addition. The characterization results showed that (1) the entry of cerium ions into the manganese oxide lattice led to the change of crystal structure of the catalyst surface and the decrease of specific surface area and pore volume; (2) the decrease of Mn^{4+} and the increase of Mn^{3+} on the catalyst surface were beneficial to the NO oxidation; (3) Ce doping increased the lattice oxygen content on the surface of the $Mn_{0.4}Ce_{0.05}$/Al, which was favorable for NO oxidation.

Data Availability

All data, models, and code generated or used during the study appear in the submitted article.

Conflicts of Interest

The authors declared no potential conflicts of interest with respect to the research, authorship, and/or publication of this article.

Acknowledgments

The present work was supported by the National Natural Science Foundation of China (51906193).

References

[1] C. Zhou, Y. Wang, Q. Jin, Q. Chen, and Y. Zhou, "Mechanism analysis on the pulverized coal combustion flame stability and NO_x emission in a swirl burner with deep air staging," *Journal of the Energy Institute*, vol. 92, no. 2, pp. 298–310, 2019.

[2] X. Jin and Y. Zhou, "Numerical analysis on microscopic characteristics of pulverized coal moderate and intense low-oxygen dilution combustion," *Energy & Fuels*, vol. 29, no. 5, pp. 3456–3466, 2015.

[3] S. Li, Y. Ge, and X. Wei, "Modeling NO and SO_2 oxidation by H_2O_2 in coal-fired flue gas," *Journal of Environmental Engineering*, vol. 144, no. 11, p. 04018113, 2018.

[4] S. Li, Y. Ge, and X. Wei, "Experiment on NO_x reduction by advanced reburning in cement precalciner," *Fuel*, vol. 224, pp. 235–240, 2018.

[5] G. Madia, M. Koebel, M. Elsener, and A. Wokaun, "The effect of an oxidation precatalyst on the NO_x reduction by ammonia SCR," *Industrial & Engineering Chemistry Research*, vol. 41, pp. 3512–3517, 2002.

[6] G. Madia, M. Elsener, M. Koebel, F. Raimondi, and A. Wokaun, "Thermal stability of vanadia tungsta-titania catalysts in the SCR process," *Applied Catalysis B: Environmental*, vol. 39, pp. 181–190, 2002.

[7] P. Glarborg, J. A. Miller, B. Ruscic, and S. J. Klippenstein, "Modeling nitrogen chemistry in combustion," *Progress in Energy and Combustion Science*, vol. 67, pp. 31–68, 2018.

[8] Y. Song, H. Hashemi, J. M. Christensen, C. Zou, P. Marshall, and P. Glarborg, "Ammonia oxidation at high pressure and intermediate temperatures," *Fuel*, vol. 181, pp. 358–365, 2016.

[9] M. H. Kim and S. W. Park, "Selective reduction of NO by NH_3 over Fe-zeolite-promoted V_2O_5-WO_3/TiO_2-based catalysts: great suppression of N_2O formation and origin of NO removal

activity loss," *Catalysis Communications*, vol. 86, pp. 82–85, 2016.

[10] M. H. Kim and H. S. Lee, "Effect of Fe-zeolite on formation of N_2O in selective reduction of NO by NH_3 over V_2O_5–WO_3/TiO_2 catalyst," *Research on Chemical Intermediates*, vol. 42, no. 1, pp. 171–184, 2015.

[11] W. Wang, R. Guo, W. Pan, and G. Hu, "Low temperature catalytic oxidation of NO over different-shaped CeO_2," *Journal of Rare Earths*, vol. 36, pp. 588–593, 2018.

[12] Z. Zhang, J. D. Atkinson, B. Jiang, M. J. Rood, and Z. Yan, "Nitric oxide oxidation catalyzed by microporous activated carbon fiber cloth: an updated reaction mechanism," *Applied Catalysis B: Environmental*, vol. 148-149, pp. 573–581, 2014.

[13] H. Wang, H. Chen, Y. Wang, and Y.-K. Lyu, "Performance and mechanism comparison of manganese oxides at different valence states for catalytic oxidation of NO," *Chemical Engineering Journal*, vol. 361, pp. 1161–1172, 2019.

[14] S. Cui, R. Hao, and D. Fu, "Integrated method of non-thermal plasma combined with catalytical oxidation for simultaneous removal of SO_2 and NO," *Fuel*, vol. 246, pp. 365–374, 2019.

[15] H. Yuan, J. Chen, H. Wang, and P. Hu, "Activity trend for low-concentration NO oxidation at room temperature on rutile-type metal oxides," *ACS Catalysis*, vol. 8, pp. 10864–10870, 2018.

[16] H. Yuan, J. Chen, Y. Guo, H. Wang, and P. Hu, "Insight into the superior catalytic activity of MnO_2 for low-content NO oxidation at room temperature," *The Journal of Physical Chemistry C*, vol. 122, pp. 25365–25373, 2018.

[17] X. Yao, J. Liu, and W. Wang, "Influence of B-site transition metal on NO oxidation over $LaBO_3$ (B=Mn, Fe and Co) perovskite catalysts," *AIP Advances*, vol. 8, p. 115222, 2018.

[18] S. Thampy, Y. Zheng, S. Dillon et al., "Superior catalytic performance of Mn-mullite over Mn-perovskite for NO oxidation," *Catalysis Today*, vol. 310, pp. 195–201, 2018.

[19] Y. Song and L. C. Grabow, "Activity trends for catalytic CO and NO co-oxidation at low temperature diesel emission conditions," *Industrial & Engineering Chemistry Research*, vol. 57, pp. 12715–12725, 2018.

[20] C. Shi, H. Chang, C. Wang et al., "Improved activity and H_2O resistance of Cu-modified MnO2Catalysts for NO oxidation," *Industrial & Engineering Chemistry Research*, vol. 57, no. 3, pp. 920–926, 2018.

[21] H. Chen, Y. Wang, and Y.-K. Lyu, "High catalytic activity of Mn-based catalyst in NO oxidation at low temperature and over a wide temperature span," *Molecular Catalysis*, vol. 454, pp. 21–29, 2018.

[22] Z. An, Y. Zhuo, C. Xu, and C. Chen, "Influence of the TiO_2 crystalline phase of MnO_x/TiO_2 catalysts for NO oxidation," *Chinese Journal of Catalysis*, vol. 35, no. 1, pp. 120–126, 2014.

[23] P. S. Metkar, V. Balakotaiah, and M. P. Harold, "Experimental and kinetic modeling study of NO oxidation: comparison of Fe and Cu-zeolite catalysts," *Catalysis Today*, vol. 184, pp. 115–128, 2012.

[24] Z. Wu, N. Tang, L. Xiao, Y. Liu, and H. Wang, "$MnO(_x)$/-$TiO(_2)$ composite nanoxides synthesized by deposition-precipitation method as a superior catalyst for NO oxidation," *Journal of Colloid and Interface Science*, vol. 352, no. 1, pp. 143–148, 2010.

[25] B.-Z. Sun, X.-L. Xu, W.-K. Chen, and L.-H. Dong, "Theoretical insights into the reaction mechanisms of NO oxidation catalyzed by Cu_2O(1 1 1)," *Applied Surface Science*, vol. 316, pp. 416–423, 2014.

[26] Z. Wang, F. Lin, S. Jiang et al., "Ceria substrate-oxide composites as catalyst for highly efficient catalytic oxidation of NO by O_2," *Fuel*, vol. 166, pp. 352–360, 2016.

[27] B.-L. Wang, J. Zhang, and H.-X. Zhong, "Effect of Ce doping content on catalytic performance of supported Co/ZrO_2 catalysts for combustion of methane," *Modern Chemical Industry*, vol. 40, no. 12, pp. 151–155, 2020.

[28] X.-H. Li, S.-L. Zhang, Y. Jia, X. Liu, and Q. Zhong, "Selective catalytic oxidation of NO with O_2 over Ce- doped MnO_x/TiO_2 catalysts," *Journal of Natural Gas Chemistry*, vol. 21, no. 1, pp. 17–24, 2012.

[29] J. Zhou, L. Yu, M. Sun et al., "MnO_2 nanosheet-assisted hydrothermal synthesis of β-MnO_2 branchy structures," *Materials Letters*, vol. 79, pp. 288–291, 2012.

[30] L. Qiu, J.-J. Meng, and D.-D. Pang, "Reaction and characterization of Co and Ce doped Mn/TiO_2 catalysts for low-temperature SCR of NO with NH_3," *Catalysis Letters*, vol. 145, no. 7, pp. 1500–1509, 2015.

[31] I. Atribak, A. Bueno-López, A. García-García, P. Navarro, D. Frías, and M. Montes, "Catalytic activity for soot combustion of birnessite and cryptomelane," *Applied Catalysis B: Environmental*, vol. 93, no. 3-4, pp. 267–273, 2010.

[32] Z. Wu, R. Jin, Y. Liu, and H. Wang, "Ceria modified MnO_x/-TiO_2 as a superior catalyst for NO reduction with NH_3 at low-temperature," *Catalysis Communications*, vol. 9, no. 13, pp. 2217–2220, 2008.

[33] J. Xiang, L.-L. Wang, F. Cao et al., "Adsorption properties of NO and NH_3 over MnO_x based catalyst supported on γ-Al_2O_3," *Chemical Engineering Journal*, vol. 302, pp. 570–576, 2016.

[34] M. Lykaki, E. Pachatouridou, S. A. C. Carabineiro et al., "Ceria nanoparticles shape effects on the structural defects and surface chemistry: implications in CO oxidation by Cu/CeO_2 catalysts," *Applied Catalysis B: Environmental*, vol. 230, pp. 18–28, 2018.

[35] Y. Cui and W.-L. Dai, "Support morphology and crystal plane effect of Cu/CeO2nanomaterial on the physicochemical and catalytic properties for carbonate hydrogenation," *Catalysis Science & Technology*, vol. 6, no. 21, pp. 7752–7762, 2016.

[36] X.-L. Guo and R.-X. Zhou, "A new insight into the morphology effect of ceria on CuO/CeO_2 catalysts for CO selective oxidation in hydrogen-rich gas," *Catalysis Science & Technology*, vol. 6, pp. 3862–3871, 2016.

[37] C. Wang, Q.-P. Cheng, X.-L. Wang et al., "Enhanced catalytic performance for CO preferential oxidation over CuO catalysts supported on highly defective CeO_2 nanocrystals," *Applied Surface Science*, vol. 422, no. 15, pp. 932–943, 2017.

[38] L. Jiang, Q. Liu, G. Ran et al., "V_2O_5-modified Mn-Ce/AC catalyst with high SO_2 tolerance for low-temperature NH_3-SCR of NO," *Chemical Engineering Journal*, vol. 370, pp. 810–821, 2019.

[39] K. Li, X. Tang, H. Yi, P. Ning, D. Kang, and C. Wang, "Low-temperature catalytic oxidation of NO over Mn-Co-Ce-Ox catalyst," *Chemical Engineering Journal*, vol. 192, pp. 99–104, 2012.

[40] H.-X. Jiang, J. Zhao, and D.-Y. Jiang, "Hollow MnO_x-CeO_2 nanospheres prepared by a green route: a novel low-temperature NH3-SCR catalyst," *Catalysis Letters*, vol. 114, no. 2, article S0169433217316616, pp. 325–332, 2014.